

Searching for an Intermediate Mass Black Hole in the Blue Compact Dwarf galaxy MRK 996

A. Georgakakis¹, Y. G. Tsamis^{2,3}, B. L. James⁴, A. Aloisi⁴

¹*National Observatory of Athens, V. Paulou & I. Metaxa, 11532, Greece.*

²*European Southern Observatory, Karl-Schwarzschild-Str. 2, 85748, Garching, Germany.*

³*Department of Physics and Astronomy, The Open University, Walton Hall, Milton Keynes, MK7 6AA, UK.*

⁴*Space Telescope Science Institute, 3700 San Martin Drive, Baltimore, MD 21218, USA.*

29 September 2010

ABSTRACT

The possibility is explored that accretion on an intermediate mass black hole contributes to the ionisation of the interstellar medium of the Compact Blue Dwarf galaxy MRK 996. Chandra observations set tight upper limits (99.7 per cent confidence level) in both the X-ray luminosity of the posited AGN, $L_X(2 - 10 \text{ keV}) < 3 \times 10^{40} \text{ erg s}^{-1}$, and the black hole mass, $\lesssim 10^4 \lambda^{-1} M_\odot$, where λ is the Eddington ratio. The X-ray luminosity upper limit is insufficient to explain the high ionisation line [OIV] $25.89 \mu\text{m}$, which is observed in the mid-infrared spectrum of the MRK 996 and is proposed as evidence for AGN activity. This indicates that shocks associated with supernovae explosions and winds of young stars must be responsible for this line. It is also found that the properties of the diffuse X-ray emission of MRK 996 are consistent with this scenario, thereby providing direct evidence for shocks that heat the galaxy's interstellar medium and contribute to its ionisation.

Key words: galaxies: individual: Markarian 996 – galaxies: active – galaxies: dwarf – X-rays: galaxies

1 INTRODUCTION

Understanding how supermassive black holes (SBH) grow and how they relate to the formation of their host galaxies are challenges for modern astrophysics. Black holes with masses $\approx 10^9 M_\odot$ have now been observed out to $z \approx 6$, when the Universe was only about 1 Gyr old (e.g. Fan et al. 2006). Simulations can produce such monsters at early epochs by postulating violent high accretion rate events triggered by mergers of gas rich galaxies (e.g. Volonteri & Rees 2005). These simulations however, have to assume seed black holes, which form very early in the Universe ($z \approx 20$) and which will eventually grow to masses as high as $10^9 M_\odot$ via accretion. The mass distribution of the seed black holes is an important parameter of the simulations. The remnants of the first stars that formed in the Universe (Population III) are believed to produce black holes with masses up to $10^3 M_\odot$ (Abel et al. 2000; Bromm et al. 2002). In this case however, accretion well in excess of the Eddington rate is required to grow those seeds to $\approx 10^9 M_\odot$ in less than 1 Gyr (e.g. Volonteri & Rees 2005; Begelman et al. 2006). An alternative scenario for the formation of seed black holes is the direct collapse of pre-galactic gas discs (Lodato & Natarajan 2006, 2007). This model produces black holes with masses up to $10^6 M_\odot$, orders of magnitude more massive than Population III stars, thereby significantly relaxing the requirements for super-Eddington accretion. A powerful probe of the seed black hole population at early

epochs are intermediate mass black holes ($\lesssim 10^6 M_\odot$) in the local Universe, which are expected to reside in low mass galaxies (i.e. $M_{BH} - \sigma$ relation; Ferrarese & Merritt 2000; Gebhardt et al. 2000; Greene et al. 2010). Volonteri et al. (2008) for example, argue that the black hole occupation number of dwarf galaxies can constrain models of the origin of the seed black holes in the early Universe, e.g. Population III stars vs direct collapse of pre-galactic gas discs.

The dynamical signatures of moderate size black holes are hard to detect with current instrumentation. As a result searches for such objects in nearby galaxies have turned to the easier but less direct approach of finding AGN in small or bulgeless galaxies, i.e. black holes during their active stage. NGC 4395 and POX 52 are the best studied examples of nearby broad-line AGN with estimated black holes mass of about $10^5 M_\odot$ (Filippenko & Ho 2003; Barth et al. 2004; Peterson et al. 2005). Furthermore, optical spectroscopic studies have recently found evidence for type-2 AGN activity associated with intermediate mass black holes in the late type spirals NGC 1042 (Seth et al. 2008; Shields et al. 2008), UGC 6192 (Barth et al. 2008) and NGC 3621 (Barth et al. 2009). Systematic efforts to compile samples of moderate size black holes have also been carried out by Greene & Ho (2004, 2007) and Dong et al. (2007). Those studies used the SDSS spectroscopic database to identify galaxies with AGN signatures in their optical spectra and

estimated black hole masses of $< 10^6 M_{\odot}$. The hosts of those AGN are typically late-type galaxies with stellar masses $< 10^{10} M_{\odot}$.

A special class of low mass galaxies which have attracted much attention over the years are Blue Compact Dwarfs (BCDs). These systems are exceptional because of their low metallicities (1/40–1/3 solar) and high specific star-formation rates, which indicate one of the first major episodes of star-formation. BCDs are therefore unique laboratories for testing theories of galaxy formation. They resemble the first galaxies that formed in the early Universe out of gas with near-primordial metallicity, and which according to the standard hierarchical formation paradigm are the building blocks of massive galaxies. An important recent development in the study of BCDs has been the suggestion that they harbor AGN associated with intermediate mass black holes. If true, this would offer the opportunity to study in detail the parallel formation of the first stars and the seed black holes in systems that resemble proto-galaxies.

Evidence for AGN activity in BCDs include, the incidence of dense ionised cores ($> 10^4 \text{ cm}^{-3}$), broad Balmer emission lines with widths in excess of 2000 km s^{-1} (Izotov et al. 2007; Izotov & Thuan 2008), high ionisation narrow optical emission lines suggesting the presence of a hard ionising continuum (Thuan & Izotov 2005; James et al. 2009). The evidence for AGN in BCDs however, is far from conclusive. Broad and high excitation lines can be due to stellar activity, e.g. shocks in fast winds of young massive stars (e.g. Izotov et al. 2007; Thuan et al. 2008; James et al. 2009). Unfortunately, optical emission line diagnostic diagrams (e.g. Baldwin et al. 1981; Kewley et al. 2001), which have traditionally been used to separate stellar photoionization-dominated from AGN-excited sources, break down at the low metallicity regime (Groves et al. 2006), and hence cannot be applied to BCDs. The most reliable method for confirming or refuting the presence of an AGN in any galaxy, irrespective of metallicity, are X-ray observations. The detection of an X-ray point source at the nuclear regions of a galaxy is strong evidence for accretion on a massive compact object.

In this paper we explore the X-ray properties of MRK 996, a BCD that is among the prime candidates for hosting an AGN. Mid-IR spectroscopy of MRK 996 with Spitzer IRS shows the [OIV] $25.89 \mu\text{m}$ line with an ionisation potential of 54.9 eV, indicating the presence of a hard continuum (Thuan et al. 2008), which could be produced by an AGN. Optical integral field spectroscopy by VLT/VIMOS have revealed an extremely dense nuclear region (electron density $\approx 10^7 \text{ cm}^{-3}$), much denser than in typical BCDs (James et al. 2009). Also, a very red point source ($J - K = 1.8$) was found at the nucleus of the galaxy, while photometry with Spitzer indicates hot dust in the central galaxy regions and a mid-IR Spectral Energy Distribution (SED) similar to that of Seyferts (Thuan et al. 2008). New Chandra observations of MRK 996 are presented in this paper and are used to search for AGN signatures in this galaxy. We adopt a distance of 22.3 Mpc for MRK 996, which corresponds to a velocity of 1642 km s^{-1} (James et al. 2009) and $H_0 = 73.5 \text{ km s}^{-1} \text{ Mpc}^{-1}$.

2 DATA PROCESSING

MRK 996 was observed for a total of 50 ks with the ACIS-S (Advanced CCD Imaging Spectrometer) camera aboard Chandra in August 3, 2009. The ACIS-S was operated in very faint mode and the target was placed at the nominal aimpoint of the S3 CCD. The data were reduced using the Chandra Interactive Analysis of Observations (CIAO) package version 4.1.2 and the methodology de-

scribed in Laird et al. (2009). The first step was to produce the level 2 event file from the raw data. Hot pixels and cosmic ray afterglows were flagged. The charge-transfer inefficiency (CTI) and time-dependent gain corrections were then applied and the ACIS pixel randomization was removed. As MRK 996 was observed in very faint mode, the ACIS particle background cleaning algorithm was also applied. The data were inspected for high particle background periods and it was found that they were not affected. Images were constructed in four energy bands 0.5–7.0 keV (full), 0.5–2.0 keV (soft), 2.0–7.0 keV (hard) and 4.0–7.0 keV (ultra-hard). Sources were detected using the methodology described in Laird et al. (2009). The final source list consists of sources with Poisson probabilities $< 4 \times 10^{-6}$ in at least one of the energy bands defined above. Source free background maps and sensitivity maps were also constructed as described in Georgakakis et al. (2008).

The astrometry of the Chandra data was refined by comparing the positions of X-ray sources with those of optical galaxies in the HST Wide Field Planetary Camera 2 (WFPC2) observations presented by Thuan et al. (1996). The astrometric accuracy of the HST image is 0.25 arcsec. Excluding sources within the optical radius of MRK 996 (0.3 arcmin) obtained from the Third Reference Catalogue of Bright Galaxies (RC3; de Vaucouleurs et al. 1991), there are only 2 X-ray sources within the HST/WFPC2 field of view. Both of them are associated with optical galaxies. Comparison of the optical and X-ray source positions shows small systematic offsets of $\delta\text{RA} = 0.25 \text{ arcsec}$ and $\delta\text{DEC} = 0.05 \text{ arcsec}$, which were applied to the X-ray source catalogue and images.

3 X-RAY POINT SOURCES

At the Poisson probability threshold of 4×10^{-6} , two X-ray point sources are detected within the optical radius of MRK 996 (0.3 arcmin). Figure 1 (left) overplots the positions of the two sources on the HST image of MRK 996. None of them is associated with the nucleus of the galaxy. Relative to the optical centre of MRK 996, one of the point sources lies $\approx 7 \text{ arcsec}$ to the south and the other $\approx 6 \text{ arcsec}$ to the north. The southern X-ray detection is likely associated with one of the globular clusters of MRK 996. It lies $\approx 0.15 \text{ arcsec}$ from an optical point source on the HST image of the galaxy identified as a globular cluster by Thuan et al. (1996).

The X-ray fluxes and luminosities of the two point sources are estimated from their X-ray spectra. The SPEXTRACT task of CIAO was employed to extract the counts at the positions of each source, estimate background spectra, generate the Redistribution Matrix Function (RMF) and the Ancillary Response File (ARF). Source spectra were grouped to have at least one count per bin. The spectral analysis was carried out within the XSPEC v12 package. As the net counts are low for both sources (see Table 1), we fit the data with a simple power-law model absorbed by cold gas in our Galaxy. A Galactic hydrogen column density of $N_{\text{H}} = 4 \times 10^{20} \text{ cm}^{-2}$ was adopted using the HI map of Kalberla et al. (2005). In XSPEC terminology, our model is $\text{wabs} \times \text{po}$, where wabs is the cold absorption from our Galaxy and po is the power-law. The derived parameters are listed in Table 1. The luminosities of the two sources are typical of X-ray binaries in galaxies.

We assess the probability that the two off-nuclear X-ray sources are background AGN. We use the 0.5–10 keV $\log N - \log S$ relation of Georgakakis et al. (2008) to estimate the expected number of sources brighter than $10^{-15} \text{ erg s}^{-1} \text{ cm}^{-2}$ within a radius of $\approx 7 \text{ arcsec}$ from the optical centre of MRK 996. The flux limit above corresponds to the approximate 0.5–10 keV flux of the

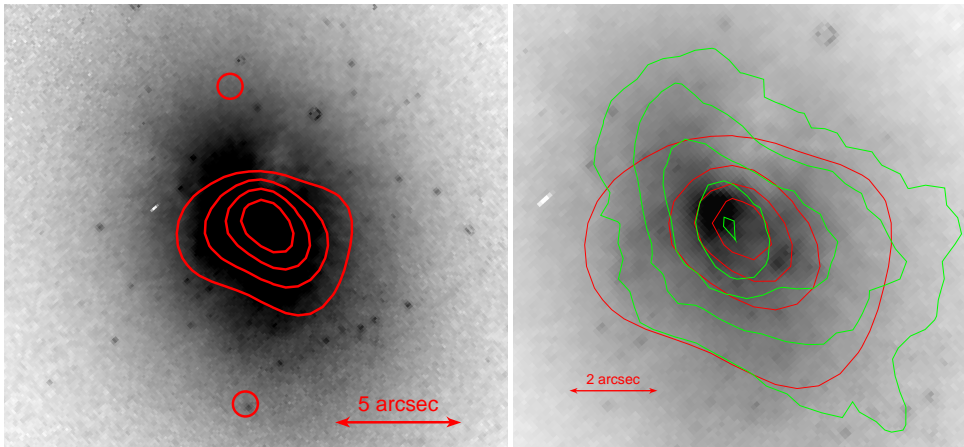


Figure 1. **Left:** HST F569W filter image of MRK 996. The circles are 0.5 arcsec in radius and mark the positions of the X-ray point sources detected in the Chandra observations. The contours correspond to the diffuse X-ray emission of MRK 996. North is up, East is left. **Right:** Zoom in the nuclear regions of MRK 996 to compare the spatial distributions of the hot X-ray emitting gas versus the optically detected H II gas. The greyscale is the HST F569W filter image, the red contours correspond to the diffuse X-ray component (same as contours on the left image) and the green contours are the narrow component of the H α emission line from the integral field spectroscopic observations described by James et al. (2009).

faintest of the two sources. The radius cut is the maximum angular distance of the two point sources from the galaxy centre. The expected number of background sources is 0.12. The Poisson probability of two background AGN within ≈ 7 arcsec of the MRK 996 nuclear regions is 1.8×10^{-4} . We conclude that both X-ray point sources are likely to be associated with MRK 996.

4 DIFFUSE EMISSION

The nuclear regions of the MRK 996 are dominated by diffuse X-ray emission. We explore the morphology of the X-ray gas by first removing point sources and then adaptively smoothing the full band X-ray image using the CMOOTH task of CIAO. The X-ray contours of the smoothed image are overplotted on the HST observations in Figure 1. The peak of the diffuse X-ray emission lies in between the nuclear star-forming region and a point source in the SW which was proposed to be a young star cluster by Thuan et al. (1996). There is also tentative evidence, limited by small photon statistics, that the distribution of the diffuse component is more extended in the southern direction. This is interesting, if it is confirmed by deeper X-ray observations, as the spatial distribution of globular clusters of MRK 996 also appears to be assymetric in the same direction. Most of them are found in the south of the galaxy (Thuan et al. 1996). Figure 1 (right) also shows that the spatial distribution of the diffuse X-ray component and the H II ionised gas are similar.

The X-ray spectrum of the diffuse component has been extracted using SPEXTRACT task of CIAO which is the proposed tool in the case of extended sources. The extraction aperture has a radius of about 2 arcsec and encompasses most of the diffuse component photons. The background spectrum was determined from nearby source-free regions. The spectrum was fit with a hot thermal plasma model Raymond & Smith (1977) which is absorbed by cold gas in our Galaxy with an HI column density of $N_{\text{H}} = 4 \times 10^{20} \text{ cm}^{-2}$. The X-ray spectrum and the best-fit model are shown in Figure 2. Table 2 lists the hot gas parameters estimated from the best-fit model to the data. The temperature of the thermal plasma, about 1 keV ($\approx 10^7$ K), is higher than the typical tempera-

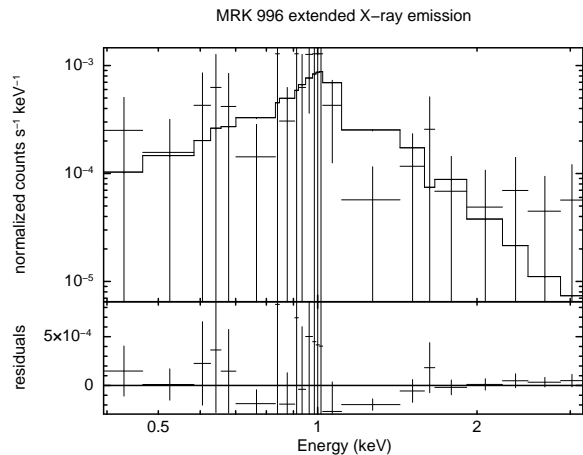


Figure 2. Spectrum of the diffuse X-ray emission of MRK 996. The best fit thermal plasma model is shown with the histogram. The residuals of the model are also plotted.

tures of the diffuse hot gas in dwarf starbursts (e.g. Ott et al. 2005) and other BCDs (Thuan et al. 2004).

5 DISCUSSION

5.1 Is there an AGN in MRK 996?

One of the motivations for the Chandra observations of MRK 996 was to explore the possibility that an AGN is responsible for the excitation of the mid-IR [OIV] 25.89 μm line reported by Thuan et al. (2008). Below about 2 keV the nuclear regions of the galaxy are dominated by diffuse hot gas, which renders the search for a point source in the soft and full bands difficult. The hard band (2-7 keV) is less contaminated by the diffuse X-ray emission. We therefore estimate a conservative upper limit (99.7 per cent confidence level) for the flux of a point source at the optical centre of MRK 996 assuming that the observed counts at that position are from a nuclear X-ray point source.

Table 1. MRK 996 point source spectral parameters. Columns are (1) CXO ID, (2) total counts within the extraction region, (3) best-fit photon index of the power-law model, (4) c-statistic value of the fit and degrees of freedom, (5) flux in the 0.3-10 keV band, (6) X-ray luminosity in the 0.3-10 keV band.

ID	Total counts	Γ	c-stat/dof	$f_X(0.3 - 10 \text{ keV})$ ($10^{-14} \text{ erg s}^{-1} \text{ cm}^{-2}$)	$L_X(0.3 - 10 \text{ keV})$ (erg s^{-1})
CXO J012735.6-061930	74	4.0 ± 0.6	33.7/24	$2.0^{+1.0}_{-0.6}$	$1.2^{+0.6}_{-0.4} \times 10^{39}$
CXO J012735.5-061943	11	$2.5^{+2.1}_{-1.6}$	8.9/9	$0.3^{+0.2}_{-0.1}$	$1.8^{+1.2}_{-0.6} \times 10^{38}$

Table 2. The gas parameters for the thermal plasma model used to fit the spectrum of the diffuse emission of MRK 996. The parameters are estimated for a metallicity $Z_{\text{opt}} = 0.5 Z_{\odot}$ determined by James et al. 2009 from the optical emission line spectrum of MRK 996 and a volume filling factor $f_v = 1$. The parameter values can be converted to lower filling factors and other metallicities using the scaling relation given in the Table, where $\xi = Z/Z_{\text{opt}}$. The listed parameters are: (1) best plasma temperature in keV, (2) the normalisation of the best-fit model, which equals $10^{-14} (4\pi D^2)^{-1} \int n_e n_H dV$, where D is the distance to MRK 996 in cm, n_e, n_H are the electron and proton densities in cm^{-3} , (3) the plasma temperature in K, (4) The 0.3-10 keV X-ray luminosity in erg/s, (5) the mean electron density in cm^{-3} estimated from the normalisation of the best-fit model assuming the proton and electron densities are equal, (6) pressure of the hot gas estimated from the relation $P/k = 2n_e T$, (7) the gas thermal energy, $E_{th} = 3n_e V kT$, where V is the volume of the X-ray emitting region, which is assumed to be a sphere of 2 arcsec=214 pc radius at the source distance (i.e. similar to the extraction region of the X-ray spectrum of the diffuse component), (8) total mass of the hot gas estimated from the relation $M_{hot} = n_e m_p V$, where m_p is the proton mass, (9) gas cooling time, $t_{cool} = E_{th}/L_X$ and (10) X-ray emissivity estimated from the relation $\Lambda_X = L_X / (norm \times 4\pi D^2 \times 10^{14})$.

Parameter	Value
kT (keV)	$1.1 \pm^{+0.4}_{-0.2}$
$norm$ (10^{-6})	$1.8^{+0.9}_{-0.7}$
T (10^7 K)	$1.3 \pm^{+0.5}_{-0.2}$
$L_X(0.3 - 10 \text{ keV})$ (10^{38} erg/s)	$1.1 \pm^{+0.6}_{-0.4}$
$\langle n_e \rangle [\times (f\xi)^{-0.5}]$ (cm^{-3})	$0.10^{+0.03}_{-0.02}$
$P/k [\times (f_v \xi)^{-0.5}]$ (10^6 K cm^{-3})	$2.7^{+1.4}_{-0.7}$
$E_{th} [\times f_v^{0.5} \xi^{-0.5}]$ (10^{53} erg)	$5.2^{+3.6}_{-1.9}$
$M_{hot} [\times f_v^{0.5} \xi^{-0.5}]$ ($10^5 M_{\odot}$)	$0.8^{+0.3}_{-0.2}$
$t_{cool} [\times f_v^{0.5} \xi^{-0.5}]$ (10^8 yr)	$1.5^{+1.1}_{-0.4}$
Λ ($10^{-23} \text{ erg s}^{-1} \text{ cm}^3$)	$1.0^{+0.7}_{-0.5}$

For the estimation of the upper limits we adopt a Bayesian methodology similar to that described in Laird et al. (2009). For a source with observed number of total counts N (source and background) within the 70 per cent EEf (Encircled Energy Fraction) radius and a local background value B the probability of flux f_X is

$$P(f_X, N) = \frac{T^N e^{-T}}{N!}, \quad (1)$$

where $N = S + B$ and $S = f_X \times t_{exp} \times C \times \eta$. In the last equation

t_{exp} is the exposure time at a particular position after accounting for instrumental effects (i.e. exposure map), C is the conversion factor from flux to count rate which depends on the adopted model for the spectrum of the source and η is the encircled energy fraction, i.e. 0.7 in our case. The integral of $P(f_X, N)$ gives the probability that the flux of the source is lower than $f_{X,U}$, i.e. the confidence interval CL for the flux upper limit

$$\int_{f_{X,L}}^{f_{X,U}} P(f_X, N) df_x = CL. \quad (2)$$

The lower limit of the integration is $f_{X,L} = 10^{-18} \text{ erg s}^{-1} \text{ cm}^{-2}$. Equation 2 is then solved numerically to estimate the flux upper limit that corresponds to the confidence interval of 99.7 per cent. For the flux to count rate conversion factor we adopt two extreme values. The first corresponds to a power-law with $\Gamma = 1.9$ and represents the case of an unabsorbed AGN. The second is for a reflection dominated spectrum, which is approximated by the PEXRAV model of XSPEC (Magdziarz & Zdziarski 1995) and represents the case of a Compton Thick AGN ($N_H \gtrsim 10^{24} \text{ cm}^{-2}$). The 99.7 per cent upper limit is $f_X(2 - 10 \text{ keV}) = 6 \times 10^{-15} \text{ erg s}^{-1} \text{ cm}^{-2}$ for the $\Gamma = 1.9$ model and $10^{-14} \text{ erg s}^{-1} \text{ cm}^{-2}$ for the reflection dominated spectrum. The 2–10 keV luminosity 99.7 per cent upper limits are respectively, 3.5×10^{38} and $6 \times 10^{38} \text{ erg s}^{-1}$. In the case of a reflection dominated spectrum, we assume that the intrinsic luminosity of the source is 50 times higher ($3 \times 10^{40} \text{ erg s}^{-1}$), as the reflected emission is believed to represent 2 per cent of the direct component (e.g. Gilli et al. 2007). The corresponding upper limits for the black hole mass are $\lesssim 100 \lambda^{-1} M_{\odot}$ in the case of no obscuration and $\lesssim 10^4 \lambda^{-1} M_{\odot}$ for Compton thick obscuring clouds, where λ is the Eddington ratio. In this calculation a bolometric to hard X-ray luminosity ratio of 35 is adopted (Elvis et al. 1994).

The luminosity upper limits above should be compared with the AGN luminosity required to explain the [OIV] 25.89 μm line in the mid-IR spectrum of MRK 996 reported by Thuan et al. (2008). Those authors modeled this line with an AGN ionization spectrum of the form $f_{\nu} \propto \nu^{-1}$ and estimated a total rate of ionizing photons $\log Q(H) = 51.125$. Assuming the photons are distributed in the energy interval 1–1000 Ry, this rate translates to a 2–10 keV intrinsic AGN luminosity of $4.5 \times 10^{40} \text{ erg s}^{-1}$. This is 2 dex higher than the 99.7 luminosity upper limit in the case of an unabsorbed AGN. This indicates that an unabsorbed or mildly absorbed active SBH cannot be responsible for the ionisation of the [OIV] 25.89 μm line. If the central engine in MRK 996 is absorbed by Compton Thick material and the X-ray emission is dominated by the reflected component, the estimated 99.7 per cent upper limit for the intrinsic luminosity of the AGN is still lower compared to that required to explain the [OIV] 25.89 μm line. We conclude that the X-ray data provide evidence against AGN ionisation for the [OIV] 25.89 μm line at a significance level of about 99.7 per cent.

5.2 Origin of the diffuse component

An alternative explanation for the [OIV] 25.89 μm line is ionisation via shocks (Thuan et al. 2008) associated with stellar outflows and supernovae explosions. Shock excitation has already been proposed to partly explain the broad component of the optical emission lines in MRK 996 (James et al. 2009). The shocks generated by starburst winds are also known to carve bubbles of hot ($10^6 - 10^7$ K) and overpressured gas in the inter-stellar medium, which can be observed at soft X-rays (e.g. Ott et al. 2005).

We explore the possibility of a superbubble for the observed diffuse X-ray emission by comparing the observed X-ray luminosity of the hot gas, as determined from the X-ray spectral analysis of section 4, with the predictions of the bubble models of Castor et al. (1975), Weaver et al. (1977), Mac Low & McCray (1988)

$$L_X = \int_0^{R_{max}} n(r)^2 \Lambda_X(T, Z) dV, \quad (3)$$

where $\Lambda_X(T, Z)$ is the X-ray volume emissivity of the gas and $n(r)$ is the radial density profile of the bubble. Substituting in the integral above the $n(r)$ relation of Chu et al. (1995) and the $\Lambda_X(T, Z)$ estimated from the observations (see Table 2) we find

$$L_X = 2.6 \times 10^{34} I L_{37}^{33/35} n_0^{17/35} t_6^{19/35} \text{ (erg s}^{-1}\text{)}, \quad (4)$$

where L_{37} is the mechanical luminosity of the starburst in units of $10^{37} \text{ erg s}^{-1}$, n_0 is the number density of the ambient ISM in cm^{-3} and t_6 is the age of the starburst in Myrs. The dimensionless integral I has a value of about 2 (see Chu et al. 1995). We do not include an explicit dependence on metallicity in equation 4 as in Chu et al. (1995). Such a dependence is accounted for in the calculation of $\Lambda_X(T, Z)$ through the normalisation of the thermal plasma model fit to the spectrum of the diffuse X-ray component.

For the estimation of the mechanical luminosity injected by the winds of young stars and supernovae explosions we use the STARBURST99 stellar evolution synthesis model (Leitherer et al. 1999; Vázquez & Leitherer 2005). We adopt a continuous star-formation model for the starburst with a Salpeter IMF (lower mass $1 M_\odot$, upper mass $100 M_\odot$, slope 2.35) and star-formation rate of $1 M_\odot \text{ yr}^{-1}$ and metallicity $Z = 0.008$, i.e. similar to the $0.5 Z_\odot$ metallicity of MRK 996 (James et al. 2009). The model mechanical luminosity is then scaled to the star-formation rate of MRK 996, for which we adopt the value $1.3 M_\odot \text{ yr}^{-1}$. This was estimated from the integral field spectroscopy observations presented by James et al. (2009) by integrating the narrow line component of the $\text{H}\alpha$ emission line under the assumption that the broad component of this line is associated with shocks. James et al. (2009) estimated an age for the young stellar population in MRK 996 of 3-5 Myr based on the equivalent width of the $\text{H}\beta$ line. An average starburst age of 4 Myr is adopted in equation 4. Under those assumptions the mechanical luminosity from the STARBURST99 model is $3.9 \times 10^{40} \text{ erg s}^{-1} \text{ cm}^{-2}$ (Figure 112 of Leitherer et al. 1999). For the density of the ambient ISM James et al. (2009) estimate $n_0 = 1 - 40 \text{ cm}^{-3}$ for the outer regions of MRK 996 based on the [S II] $\lambda 6716/\lambda 6731$ intensity ratio. In ionized nebulae however, the [S II] emission is typically associated with lower ionization gas which would be expected to be of higher density than the average. It is therefore likely that the lower end of the n_0 range determined by James et al. (2009) represents the mean ISM density into which the superbubble expands. Adopting $n_0 = 1 \text{ cm}^{-3}$ we predict an X-ray luminosity of $3 \times 10^{38} \text{ erg s}^{-1}$, larger than the observed one, $1.1 \times 10^{38} \text{ erg s}^{-1}$. However, given the large uncertainties in the model parameters (e.g. a slightly younger age of

3 Myr yields $L_X = 7 \times 10^{37} \text{ erg s}^{-1}$) and the observables (e.g. $\Lambda_X(T, Z)$, metallicity of the X-ray emitting gas, ISM density) we conclude that the observed L_X of the diffuse component is broadly consistent with the expanding bubble model prediction.

We caution that the diffuse component could be the result of the combined emission of high mass X-ray binaries (HMXRBs) that lie below the sensitivity limit of the Chandra observations. We assess the contribution of such sources by integrating the global luminosity function of HMXRBs in starburst galaxies determined by Grimm et al. (2003). A star-formation rate of $1.3 M_\odot/\text{yr}$ is adopted for MRK 996 (James et al. 2009) and the integration is carried out between 10^{37} and $10^{38} \text{ erg s}^{-1}$. The upper limit is the approximate 0.5-10 keV band point source sensitivity limit of the Chandra observations. We estimate a total X-ray luminosity for HMXRBs below the Chandra data detection threshold of $\approx 10^{39} \text{ erg s}^{-1}$. In principle the diffuse X-ray component could be attributed to HMXRBs. The X-ray spectrum of the diffuse component is not inconsistent with this interpretation. The best-fit spectral index of the power-law component is 2.2 ± 0.7 . Although HMXRBs typically have flatter X-ray spectra, ≈ 1.2 (e.g. White et al. 1983), systems with spectral indices as flat as $\Gamma \approx 2$ have been observed (e.g. Sasaki et al. 2003). Although it is hard to reject the possibility of X-ray binaries dominating the diffuse component there are arguments against this interpretation. The age of the starburst in MRK 996 is 3 – 5 Myr (James et al. 2009), while models of the evolution of the X-ray luminosity of HMXRBs (e.g. Sipior 2003; Linden et al. 2010) predict that these sources peak at later times, $\approx 10 - 20$ Myr after the initial burst, especially in the case of low metallicity systems. It is also interesting that the peak of the diffuse X-ray emission falls between the nuclear starburst and the young super-star cluster candidate in the SW of the nucleus identified by Thuan et al. (1996). One could reasonably assume that the peak emission is associated with an interaction region where the respective stellar wind super bubbles from the two sources collide and heat the ISM.

6 CONCLUSIONS

Chandra X-ray observations are used to search for an AGN in the BCD MRK 996, which could explain the high ionisation line [OIV] 25.89 μm observed in the mid-IR spectrum of the galaxy. The estimated upper limit for the X-ray luminosity of a nuclear point source in MRK 996 is inconsistent with AGN ionisation being responsible for the excitation of the [OIV] 25.89 μm line. Shock excitation must be responsible for this line. We find direct evidence for shocks by studying the diffuse X-ray emission of MRK 996. The properties of this component are broadly consistent with shock heating from stellar winds and supernovae explosions. A tight upper limit of $\lesssim 10^4 \lambda^{-1} M_\odot$ is also set for the posited black hole mass of MRK 996.

7 ACKNOWLEDGMENTS

AG acknowledges financial support from the Marie-Curie Reintegration Grant PERG03-GA-2008-230644. YGT acknowledges the award of a Marie Curie intra-European Fellowship within the 7th European Community Framework Programme (grant agreement PIEF-GA-2009-236486). Support for this work was provided by the National Aeronautics and Space Administration through Chandra Award Number 11700503 issued by the Chandra X-ray Observatory Center, which is operated by the Smithsonian Astrophysical

Observatory for and on behalf of the National Aeronautics Space Administration under contract NAS8-03060.

REFERENCES

- Abel T., Bryan G. L., Norman M. L., 2000, *ApJ*, 540, 39
- Baldwin J. A., Phillips M. M., Terlevich R., 1981, *PASP*, 93, 5
- Barth A. J., Greene J. E., Ho L. C., 2008, *AJ*, 136, 1179
- Barth A. J., Ho L. C., Rutledge R. E., Sargent W. L. W., 2004, *ApJ*, 607, 90
- Barth A. J., Strigari L. E., Bentz M. C., Greene J. E., Ho L. C., 2009, *ApJ*, 690, 1031
- Begelman M. C., Volonteri M., Rees M. J., 2006, *MNRAS*, 370, 289
- Bromm V., Coppi P. S., Larson R. B., 2002, *ApJ*, 564, 23
- Castor J., McCray R., Weaver R., 1975, *ApJ*, 200, L107
- Chu Y., Chang H., Su Y., Mac Low M., 1995, *ApJ*, 450, 157
- de Vaucouleurs G., de Vaucouleurs A., Corwin Jr. H. G., Buta R. J., Paturel G., Fouqué P., 1991, *Third Reference Catalogue of Bright Galaxies. Volume 1-3*, XI, 2069 pp. 7 figs, Springer-Verlag Berlin Heidelberg New York.
- Dong X., Wang T., Yuan W., Zhou H., Shan H., Wang H., Lu H., Zhang K., 2007, in *Astronomical Society of the Pacific Conference Series*, Vol. 373, *The Central Engine of Active Galactic Nuclei*, L. C. Ho & J.-W. Wang, ed., pp. 57–+
- Elvis M., et al., 1994, *ApJS*, 95, 1
- Fan X., et al., 2006, *AJ*, 131, 1203
- Ferrarese L., Merritt D., 2000, *ApJ*, 539, L9
- Filippenko A. V., Ho L. C., 2003, *ApJ*, 588, L13
- Gebhardt K., Bender R., Bower G., Dressler A., Faber S. M., Filippenko A. V., Green R., Grillmair C., Ho L. C., Kormendy J., Lauer T. R., Magorrian J., Pinkney J., Richstone D., Tremaine S., 2000, *ApJ*, 539, L13
- Georgakakis A., Nandra K., Laird E. S., Aird J., Trichas M., 2008, *MNRAS*, 388, 1205
- Gilli R., Comastri A., Hasinger G., 2007, *A&A*, 463, 79
- Greene J. E., Ho L. C., 2004, *ApJ*, 610, 722
- , 2007, *ApJ*, 670, 92
- Greene J. E., Peng C. Y., Kim M., Kuo C. Y., Braatz J. A., Impellizzeri C. M. V., Condon J. J., Lo K. Y., Henkel C., Reid M. J., 2010, *ArXiv e-prints*
- Grimm H., Gilfanov M., Sunyaev R., 2003, *MNRAS*, 339, 793
- Groves B. A., Heckman T. M., Kauffmann G., 2006, *MNRAS*, 371, 1559
- Izotov Y. I., Thuan T. X., 2008, *ApJ*, 687, 133
- Izotov Y. I., Thuan T. X., Guseva N. G., 2007, *ApJ*, 671, 1297
- James B. L., Tsamis Y. G., Barlow M. J., Westmoquette M. S., Walsh J. R., Cuisinier F., Exter K. M., 2009, *MNRAS*, 398, 2
- Kalberla P. M. W., Burton W. B., Hartmann D., Arnal E. M., Bajaja E., Morras R., Pöppel W. G. L., 2005, *A&A*, 440, 775
- Kewley L. J., Dopita M. A., Sutherland R. S., Heisler C. A., Trevena J., 2001, *ApJ*, 556, 121
- Laird E. S., et al., 2009, *ApJS*, 180, 102
- Leitherer C., Schaerer D., Goldader J. D., González Delgado R. M., Robert C., Kune D. F., de Mello D. F., Devost D., Heckman T. M., 1999, *ApJS*, 123, 3
- Linden T., Kalogera V., Sepinsky J. F., Prestwich A., Zezas A., Gallagher J., 2010, *arXiv1005.1639*
- Lodato G., Natarajan P., 2006, *MNRAS*, 371, 1813
- , 2007, *MNRAS*, 377, L64
- Mac Low M., McCray R., 1988, *ApJ*, 324, 776
- Magdziarz P., Zdziarski A. A., 1995, *MNRAS*, 273, 837
- Ott J., Walter F., Brinks E., 2005, *MNRAS*, 358, 1453
- Peterson B. M., Bentz M. C., Desroches L., Filippenko A. V., Ho L. C., Kaspi S., Laor A., Maoz D., Moran E. C., Pogge R. W., Quillen A. C., 2005, *ApJ*, 632, 799
- Raymond J. C., Smith B. W., 1977, *ApJS*, 35, 419
- Sasaki M., Pietsch W., Haberl F., 2003, *A&A*, 403, 901
- Seth A., Agüeros M., Lee D., Basu-Zych A., 2008, *ApJ*, 678, 116
- Shields J. C., Walcher C. J., Böker T., Ho L. C., Rix H., van der Marel R. P., 2008, *ApJ*, 682, 104
- Sipior M. S., 2003, PhD thesis, "Population synthesis and its connection to astronomical observables", The Pennsylvania State University
- Thuan T. X., Bauer F. E., Papaderos P., Izotov Y. I., 2004, *ApJ*, 606, 213
- Thuan T. X., Hunt L. K., Izotov Y. I., 2008, *ApJ*, 689, 897
- Thuan T. X., Izotov Y. I., 2005, *ApJS*, 161, 240
- Thuan T. X., Izotov Y. I., Lipovetsky V. A., 1996, *ApJ*, 463, 120
- Vázquez G. A., Leitherer C., 2005, *ApJ*, 621, 695
- Volonteri M., Lodato G., Natarajan P., 2008, *MNRAS*, 383, 1079
- Volonteri M., Rees M. J., 2005, *ApJ*, 633, 624
- Weaver R., McCray R., Castor J., Shapiro P., Moore R., 1977, *ApJ*, 218, 377
- White N. E., Swank J. H., Holt S. S., 1983, *ApJ*, 270, 711